# FUNCTIONAL OPTIMIZATION OF BROADLY NEUTRALIZING HIV-1 ANTIBODY 10E8 BY PROMOTING MEMBRANE INTERACTIONS

Running Title: Rational optimization of an anti-MPER antibody

Edurne Rujas[a*], Daniel P. Leaman[b*], Sara Insausti[a], Lei Ortigosa-Pascual[a], Lei Zhang[b], Michael B. Zwick[b#] and José L. Nieva[a#]

Biofisika Institute (CSIC, UPV/EHU) and Department of Biochemistry and Molecular Biology, University of the Basque Country (UPV/EHU), Bilbao, Spain[a] ; Department of Immunology and Microbial Science, The Scripps Research Institute, La Jolla, California, USA [b],

#Address correspondence to Jose L. Nieva, joseluis.nieva@ehu.es; or to Michael Zwick, zwick@scripps.edu.

*These authors contributed equally to this work.

word count for the abstract: **243**

word count for the "importance" section: **133**

word count for the text: **10,079**

**Abstract**

The 10E8 antibody targets a helical epitope in the membrane-proximal external region (MPER) and transmembrane domain (TMD) of the envelope glycoprotein (Env) subunit gp41, and is among the broadest known neutralizing antibodies against HIV-1. Accordingly, this antibody and its mechanism of action valuably inform the design of effective vaccines and immunotherapies. 10E8 exhibits unusual adaptations to attain specific, high-affinity binding to the MPER at the viral membrane interface. Reversing charge of the basic paratope surface (from net positive to net negative) reportedly lowered its neutralization potency. Here, we hypothesized that by increasing the net positive charge in similar polar surface-patches, the neutralization potency of the antibody may be enhanced. We found that increased positive charge at this paratope surface strengthened an electrostatic interaction between antibody and lipid bilayers, enabling 10E8 to interact spontaneously with membranes. Notably, the modified 10E8 did not gain any observable polyreactivity and neutralized with significantly greater potency. Binding analyses indicated that the optimized 10E8 bound with higher affinity to the epitope peptide anchored in lipid bilayers, and to Env spikes on virions. Overall our data provide a proof-of-principle for rational optimization of 10E8 via manipulation of its interaction with the membrane element of its epitope. However, the observation that a similar mutation strategy did not affect potency of the first-generation anti-MPER antibody 4E10, shows possible limitations of this principle. Altogether, our results emphasize the crucial role played by the viral membrane in the antigenicity of the MPER-TMD of HIV-1.

**Importance**

The broadly neutralizing antibody (bnAb) 10E8 blocks infection by nearly all HIV-1 isolates, a capacity which vaccine design seeks to reproduce. Engineered versions of this antibody also represent a promising treatment for HIV infection by passive immunization. Understanding its mechanism of action is therefore important to help develop effective vaccines and biologics to combat HIV/AIDS. 10E8 engages with its helical MPER epitope where the base of the envelope spike submerges into the viral membrane. To enable this interaction, this antibody evolved an unusual property: the ability to interact with the membrane surface. Here, we provide evidence that 10E8 can be made more effective by enhancing its interactions with membranes. Our findings strengthen the idea that to elicit antibodies similar to 10E8, vaccines must reproduce the membrane environment where these antibodies perform their function.

## Introduction

Broadly neutralizing antibodies (bnAbs) against HIV-1 have been essential tools in the design of candidate vaccines and therapeutics, from the first-generation bnAbs of the 1990s to the more potent, second-generation of bnAbs defined since 2009 (1). The second-generation bnAb 10E8 recognizes the conserved membrane-proximal external region (MPER) of the gp41 subunit of the envelope glycoprotein (Env) (2-5) resulting in one of the broadest levels of HIV-1 neutralization reported to date (1, 6-8). Antibodies against this vulnerable site also mediate neutralization breadth and potency of sera from a subset of HIV-1-infected individuals (8, 9). Despite reported similarities in the epitope binding profile with the first-generation anti-MPER bnAb 4E10, 10E8 displays higher neutralization potency, and, if any, very limited polyreactivity by comparison (8, 10). These advantageous features have put the focus on 10E8 as a suitable template on which to base vaccine design (11-14) and rational development of immunotherapeutic agents (15-20).

The antigen responsible for eliciting 10E8-like antibodies, and the molecular mechanism underlying effective MPER recognition are not totally understood. Recently published structural data suggested that the MPER and its connection to the gp41 transmembrane domain (TMD) are organized as a continuous, straight helix that emerges obliquely from the HIV membrane plane (3, 4, 21, 22). The ability to access the helical MPER epitope at the viral membrane interface thus appears to support the neutralizing activity of the most effective anti-MPER antibodies (3, 22). Structural elements of the antibody sustain effective interactions with the lipid bilayer surrounding the viral particle: i) a long heavy-chain complementarity determining region 3 (CDRH3) loop decorated at the apex with hydrophobic-at-interface aromatic residues critical for function (3, 8, 23, 24); and ii) a flat

surface at the paratope that establishes favorable interactions at the viral Env-membrane interface (4, 22, 25).

Recent studies have suggested that the association of anti-MPER antibodies with membranes might be driven by electrostatic interactions between basic residues on the surface of the paratope, and anionic phospholipids (4, 22, 25). Despite the inability of 10E8 to partition spontaneously into lipid bilayers (25), cryo-EM and x-ray crystallography data suggest that, upon engagement with antigen, a surface patch of its paratope may establish favorable contacts with the membrane Env interface (2-4). Specifically, in a recent study, anionic phospholipids have been found attached to this surface (4). These authors found that introduction of aspartate or glutamate at basic/polar positions surrounding the phospholipid binding site decreased the neutralization potency to 1/500th of that of WT 10E8 (4). Thus, the deleterious effects caused by those mutations highlighted the functional relevance of potential electrostatic interactions of 10E8 with the membrane.

Here, we followed the opposite approach; to optimize function of 10E8 by enhancing the net positive charge of its paratope. We determined the strength of antibody-membrane interactions using liposome-flotation assays (a physical separation method). This standard method was complemented with fluorescence-based assays (water-membrane partitioning in intact systems, i.e., without isolation of the bound fractions), namely, confocal microscopy of Giant Unilamellar Vesicles (GUVs) and spectroscopic titration assays. In addition, we determined whether the strength of antibody-membrane interactions was associated with polyreactivity and neutralization potency. We found that the neutralization efficacy of the 10E8 antibody was substantially improved by manipulation of antibody-membrane interactions. A similar approach taken with a first-generation bnAb, 4E10, did not improve

its potency, suggesting that factors other than membrane recognition contribute to neutralization activity. Notably, our observations do not support the proportionality between level of polyreactivity and neutralization potency. In addition, they emphasize that favorable interactions with the membrane are likely crucial to the functional antibody-antigen binding interface, and therefore highly relevant for inducing effective anti-MPER B-cell responses. Finally, in a more general sense, they suggest a possible pathway for improving the potency of antibodies targeting membrane-displayed epitopes.

## Materials and Methods

*Materials*

The peptides used in this study were synthesized in the C-terminal carboxamide form by solid-phase methods using Fmoc chemistry, purified by reverse phase high-pressure liquid chromatography, and characterized by matrix-assisted time-of-flight mass spectrometry (purity >95%). Peptides were routinely dissolved in DMSO and their concentration determined by the bicinchoninic acid microassay (Pierce, Rockford, IL, USA) or by their absorbance at 280 nm. Goat anti-human IgG-Fab antibody was purchased from Sigma (St. Louis, MO). Secondary antibody conjugated to horseradish peroxidase (HRP), mouse anti-goat IgG-HRP and rabbit anti-human IgG-HRP was purchased from Santa Cruz (Heidelberg, Germany). The fluorescent probes 6-dodecanoyl-2-dimethylaminonaphthalene (Laurdan) and 4-Chloro-7-Nitrobenz-2-Oxa-1,3-Diazole (NBD) were obtained from Molecular Probes (Eugene, OR, USA). Abberior Star 580 (KK114) was obtained from Abberior (Göttingen,

Germany). Lipids 1,2-dioleoyl-*sn*-glycero-3-phosphocholine (DOPC), 1,2-dioleoyl-*sn*-glycero-3-phosphoethanolamine (DOPE), 1,2-dioleoyl-*sn*-glycero-3-phosphoserine (DOPS), sphingomyelin (SM), cholesterol (Chol), and 1,2-dioleoyl-*sn*-glycerol-3-phosphoethanolamine-N-(lissamine rhodamine B sulfonyl) (Rho-PE) were purchased from Avanti Polar Lipids (Alabaster, Alabama).

*Production, characterization and labeling of Fabs*

Antibody sequences were cloned in the plasmid pColaDuet and expressed in *Escherichia coli* T7-shuffle strain. Recombinant expression was induced at 18°C overnight with 0.4 mM isopropyl-D-thiogalactopyranoside when the culture reached an optical density of 0.8. Cells were harvested and centrifuged at 8,000 × *g*, after which they were resuspended in a buffer containing 50 mM HEPES (pH 7.5), 500 mM NaCl, 35 mM imidazole, DNase (Sigma-Aldrich, St. Louis, MO) and an EDTA-free protease inhibitor mixture (Roche, Madrid, Spain). Cell lysis was performed using an Avestin Emulsiflex C5 homogenizer. Cell debris was removed by centrifugation, and the supernatant loaded onto a nickel-nitrilotriacetic acid (Ni-NTA) affinity column (GE Healthcare). Elution was performed with 500 mM imidazole, and the fractions containing the His-tagged proteins were pooled, concentrated and dialyzed against 50 mM sodium phosphate (pH 8.0), 300 mM NaCl, 1 mM DTT, and 0.3 mM EDTA in the presence of purified protease Tobacco etch virus (26). Fabs were separated from the cleaved peptides containing the $His_{6x}$ tag by an additional step in a Ni-nitrilotriacetic column. The flow-through fraction containing the antibody was dialyzed overnight at 4 ºC against sodium acetate (pH 5.6) supplemented with 10% glycerol and subsequently loaded onto a

MonoS ion exchange chromatography (IEC) column (GE Healthcare). Elution was carried out with a gradient of potassium chloride and the fractions containing the purified Fab concentrated and dialyzed against a buffer containing 10 mM sodium phosphate (pH 7.5), 150 mM NaCl, and 10% glycerol. For the preparation of mutant Fabs, the KOD-Plus mutagenesis kit (Toyobo, Osaka, Japan) was employed following the instructions of the manufacturer. Labeling with the polarity-sensitive NBD probe was performed as described (27, 28). In brief, a cysteine-substituted Fab derivative (W100b$_{HC}$C) was first generated by site-directed mutagenesis and modified with a sulfhydryl-specific iodoacetamide derivative of NBD. Thus, this procedure results in the conservative substitution of the Trp indole ring by the similarly bicyclic nitrobenzoxadiazole ring, which makes comparable changes in polarity scored by the NBD label. For confocal microscopy experiments, the fluorescence probe KK114 was introduced *in vitro* at position C216$_{HC}$ following the same procedure as for the NBD probe.

*Lipid vesicle production*

Large unilamellar vesicles (LUVs) made of the virus-like (VL) lipid mixture (DOPC, Chol, SM, DOPE and DOPS in a molar ratio of 14:46:17:16:7) were produced following the extrusion method (29). To that end, lipid suspensions were subjected to 10 freeze-thaw cycles prior to extrusion 10 times through 2 stacked polycarbonate membranes with a nominal pore-size of 0.1 µm (Nuclepore, Inc., Pleasanton, CA, USA). Giant unilamellar vesicles (GUVs) with the same composition were produced by spontaneous swelling following procedures described in (30, 31). Briefly, lipids were mixed in $CHCl_3$:$CH_3OH$ (9:1) and the organic

168 solvent was removed by desiccation for 1 h. Dried silica beads covered with lipid were
169 collected and transferred to a 7.5 g/L sucrose buffer to induce spontaneous swelling of GUVs.
170 For preparation of peptide-GUVs complexes, 0.66 µM peptide was added to the observation
171 dish in an isosmotic 10 mM HEPES, 150 mM KCl (pH 7.4) buffer followed by the addition
172 of the formed vesicles.

173

174 *Vesicle flotation assays.*

175 The partition of the antibody into membranes was examined by vesicle flotation experiments
176 in sucrose gradients following the method described by Yethon *et al* (32). In brief, 100 µl of
177 VL LUVs labeled with the lipid rhodamine-PE (Avanti Polar lipids, Alabaster, AL), were
178 incubated with the Fabs at 25ºC for 15 min under continuous stirring (800 r.p.m.). The
179 mixture was adjusted to a sucrose concentration of 1.4 M in a final volume of 300 µl, and
180 subsequently deposited on a stepwise gradient composed of successive solutions containing
181 0.8 M (400 µl) and 0.5 M sucrose (300 µl). The gradient was centrifuged at 4 ºC and 436,000
182 × *g* for 3 h in a TLA120.2 rotor (Beckman Coulter, Brea, CA). After centrifugation, four
183 fractions each of 250 µl were collected. The material that adhered to the centrifugation tubes
184 was extracted by washing the tubes with 250 µl of a solution of 1% (w/v) SDS at 100°C.
185 Antibody Fab fragments were detected in SDS PAGE using Western blot and the presence
186 of liposomes monitored by measuring Rhodamine fluorescence. Densitometry of the blotted
187 Fab bands was performed using ImageJ software, and the percentage of Fab bound to vesicles
188 calculated from the band intensities measured in the vesicle-floating fractions, relative to the
189 sum of intensities measured in all fractions.

*Confocal microscopy*

Images were acquired on a Leica TCS SP5 II microscope (Leica Microsystems GmbH, Wetzlar, Germany) as described (31, 33). Laurdan-stained GUVs were excited at 780 nm using a x63 water-immersion objective (numerical aperture, NA=1.2) and 512x512 pixel images were acquired at 400 Hz per scanning line and emission imaged at 435 ± 20 nm. The KK114-labeled Fabs were excited at 633 nm by HeNe laser and emission imaged at 775 ± 125 nm.

*Spectroscopic titration*

NBD fluorescence emission spectra were recorded with the excitation wavelength fixed at 470 nm. An emission spectrum of a sample lacking the fluorophore was subtracted from the spectrum of the equivalent sample containing the fluorophore. Partitioning curves were computed from the fractional changes in emitted NBD-fluorescence when 150 nM of NBD labeled Fab was titrated with increasing lipid concentrations. The mole fraction partition coefficients, $K_X$, were determined by fitting the experimental values to a hyperbolic function (34):

$$F/F_0 = 1 + \frac{[(F_{max}/F_0)-1]\,[L]}{K + [L]} \qquad [1]$$

where [L] is the concentration of accessible lipid and K is the lipid concentration at which the bound peptide fraction is 0.5. Therefore, $K_X$ = [W]/$K$ where [W] is the molar concentration of water. The observed free energy of water-membrane partitioning was subsequently calculated according to the following expression:

$$\Delta G_{obs} = -RT \ln K_x \qquad [2]$$

For the estimation of the electrical potential at the membrane surface as a function of the PS content, the following equation was used:

$$\Psi_0 = [2kT/ze] \operatorname{arcsinh} [A\sigma/(c)^{1/2}] \qquad [3]$$

where $c$ is the number of ions per volume, and $\sigma$ the surface charge density (35). To calculate the latter parameter a surface area per phospholipid of 69.5 $Å^2$ was considered, and net charges of 0 and -1 were assigned to PC and PS, respectively (36).

*HEp-2 cell immunofluorescence assay.*

Antibodies (Fabs) were assessed for the ability to stain HIV-1 negative human epithelial HEp-2 (VIRGO ANA/HEp-2) cells on glass slides by indirect immunofluorescence microscopy. Fabs were diluted to 25 µg/ml and 10 µl used for each test as per the manufacturer's specifications. FITC-conjugated goat anti-human Fab (Jackson) was used as the secondary probe. Slides were photographed using an EVOS fluorescence microscope (Invitrogen). Staining experiment #1 with 10E8-3R and experiment #2 with 4E10-3R were performed separately; intensity of antibody staining can be compared within but not between experiments.

232

233 *ELISA for antibody polyreactivity.*

234 Ninety-six-well plates were coated with 10 nM Cholesterol, DOPS, POPC or DOPE (Sigma)
235 in 50 µl 100% methanol and left to evaporate overnight at 4°C. Other antigens (500 ng/well
236 in PBS) were coated on wells overnight at 4°C without evaporation. The wells were washed
237 three times with PBS containing 0.05% Tween 20 (PBST) and blocked for 1 h at 37°C with
238 4 % non-fat dry milk in PBS. The wells were washed three times with PBST, and Fabs diluted
239 in 0.4 % NFDM-PBST were added to the wells and incubated for 2 h at 37°C. Following
240 three washes with PBST, goat anti-human Fab-HRP conjugate (1:500 in 0.4% NFDM-PBST)
241 was added to the wells and incubated for 45 min at RT. The wells were washed three times
242 with PBST and the plate was developed using TMB substrate (Pierce) at 37°C. The OD at
243 450 nm was determined using a Synergy H1 plate reader (Biotek).

244

245 *Virus production.*

246 HIV-1 pseudotyped virus was generated by co-transfection of 293T cells with Env plasmid
247 DNA and the HIV-1 backbone plasmid pSG3ΔEnv (37) using 25K polyethylene imine (PEI),
248 as previously described (38). Envs for HIV isolates JRFL, LAI, SF162 were obtained from
249 the NIH ARRRP, 92RW020, 94UG103, 92BR020, 92TH021, IAVI C22, and BG505 from
250 D. Burton (Scripps), 16055 from R. Wyatt (Scripps), COT6 from L. Morris (U.
251 Witwatersrand), Q23.17 from J. Overbaugh (Fred Hutchinson), Du422.01 and CH181.12
252 from M. Seaman (Beth Israel Deaconess Medical Center), and TAN2 from B. Hahn (U.
253 Pennsylvania). Envs were expressed from the pSVIII plasmid; Comb-mut, by exception was

contained in the pcDNA plasmid. Virions for BN-PAGE analysis were produced by transient transfection using the molecular clone, pLAI-Comb-mut (39).

*Neutralization assays.*

Neutralization was determined using a single-cycle neutralization assay with $CD4^+CXCR4^+CCR5^+$ TZM-bl cells as target cells. Antibodies were added to virus in cell culture media (DMEM supplemented with 10% FBS, 2mM L-glutamine, 100 U/mL penicillin, and 100 µg/mL streptomycin) and incubated for 1h at 37°C prior to addition to target cells. Following a 72 h incubation at 37°C, cells were lysed, Bright-Glo luciferase reagent (Promega) was added, and luminescence in relative light units (RLUs) was measured using a Synergy H1 plate reader (BioTek).

*Blue native (BN)-PAGE Western Blot.*

For BN-PAGE gel mobility shift assays, Comb-mut virions (39) were incubated with Fab fragments of antibodies at RT for 30 min. Env was solubilized from the membrane using 1% DDM in Tris-Glycine Native Sample Buffer (ThermoFisher), supplemented with 0.25% Coomassie G-250, and loaded onto a 3-8% gradient Tris-Acetate NuPAGE gel (ThermoFisher). For washout assays, following incubation with antibodies for 30 min the sample volume was increased to 1 ml using Sample Buffer and the virus was centrifuged at 21,000 RCF for 45 min at 4ºC. Supernatant containing unbound Fabs was removed and the virus pellet was resuspended in Sample Buffer and processed for BN-PAGE, as above. Electrophoresis was performed for 3 h at 150 V in Tris-Glycine Native Running Buffer (ThermoFisher) that was supplemented with 0.002% Coomassie G-250. Proteins were transferred onto a PDVF membrane using an XCell II Blot Module (ThermoFisher), and then

probed using a cocktail of antibodies to gp120 (F105, 2G12 and F425-B4e8, 2 µg/ml each) and gp41 (2F5, Z13e1 and 7B2, 1 µg/ml each). Primary antibodies were further probed using a goat anti-human-Fcγ-HRP secondary antibody (Jackson) and the blot was developed using ECL Plus Substrate (Pierce).

## Results

*Design of 10E8-3R antibody*

To engineer antibody 10E8 to interact more effectively with lipid bilayers, we introduced three basic residues (3R mutation) at strategic, solvent-exposed positions on the corresponding Fab (Fig. 1A). The triple substitution S30R/N52R/S67R, involving light chain residues, increases the positive charge at the surface patch predicted by x-ray crystallography and cryo-EM studies to contact the viral Env-membrane interface (2-4) (Figs. 1A, B). Positioning in the structure of the anionic phospholipid phosphatidylglycerol co-crystalized in complex with the Fab 10E8 (4), confirmed the close proximity of its head-group moiety to the mutated residues (Fig. 1B, right). Moreover, this arrangement of the antibody with respect to the membrane plane resulted in an insertion angle of the bound MPER helix resembling that deduced from a low-resolution cryo-EM model of 10E8 bound to the Env trimer (2). These changes did not alter binding to epitope peptide, as judged from the comparable patterns of specific binding observed for mutant and parental Fabs in ELISA (Fig. 1C). Thus, we next studied the membrane-binding characteristics and biological

functions of the resulting Fab mutant 10E8-3R, in comparison with those of the parental specimen 10E8-WT.

*Membrane binding properties of 10E8-3R*

Following the approach described in our preceding works (24, 25) (see also schematics displayed in Fig. 2A), VL vesicle flotation experiments were first used to establish the effect of the 3R mutations on Fab 10E8 partitioning from water into membranes (Fig. 2B). Anti-gp120 antibody PG9, used as a control for the absence of interaction with membranes, and 10E8-WT showed similar flotation profiles after sucrose centrifugation, with most input antibody recovered in pellets (i.e., from non-floating fractions). In sharp contrast, under the same experimental conditions, 67 % of 10E8-3R was found co-floating with vesicles (Rho emission spectra in the bottom row). Antibody signal was mainly detected in the non-floating fractions when the same experiment was run in the absence of vesicles. To ensure that the observed membrane binding phenomenon was dependent on the specific location of the 3R mutation, three Arg residues were instead placed in solvent-exposed positions S153R, S193R and S199R of the 10E8 constant domain light chain. The resultant 10E8-3R(C) mutant was found in the pellet fractions after centrifugation. Thus, the minimal amount of Fab 10E8-3R(C) detected in association with vesicles followed the pattern of the parental 10E8-WT. These results indicate that the light-chain 3R mutation S30R/N52R/S67R specifically endows 10E8 antibody with the capacity of partitioning into VL vesicles.

Assays using fluorescently labeled Fabs were additionally performed to prove the membrane-binding capacity of 10E8-3R in an intact system (i.e., without physical separation of the

vesicle-bound specimens). Figure 3A displays confocal fluorescence microscopy data of GUVs incubated with Fab. To carry out those experiments, GUVs were stained with Laurdan (emission rendered in green color), and Fabs were labeled with the probe Abberior STAR RED (KK114, rendered in red color), the latter of which was conjugated with residue $C216_{HC}$ of the constant domain. In accordance with spontaneous partitioning of the 3R mutant into bare membranes, VL GUVs incubated with the KK114-10E8-3R mutant were simultaneously stained with Laurdan and KK114. In contrast, no KK114 staining was detected in GUVs incubated with KK114-10E8-WT.

Membrane binding by 10E8-3R was also assessed using Fabs labeled with the molecular sensor 7-nitrobenz-2-oxa-1,3-diazol-4-yl (NBD) (Fig. 3B). This approach to probe protein-membrane interactions was described in our prior studies (3, 24, 25), and is based on monitoring changes in fluorescence emission that occur upon transferring the NBD probe from an aqueous solvent into the less polar environment of the lipid bilayer. The changes in NBD emission, i.e., intensity increase and blue-shift of the emission maximum wavelength, are exemplified by the model spectra displayed in Figure 3B (left panel). An observed shift of the emission maximum wavelength and an increase of the fluorescence intensity were observed in samples incubated with NBD-10E8-3R, which is consistent with a tendency of the 3R mutant to associate spontaneously with VL membranes (Fig. 3C, bottom-right). In contrast, incubation of the NBD-10E8-WT Fab with VL LUVs did not induce appreciable changes in the emitted fluorescence (Fig. 3C, bottom-left).

To confirm the contribution of electrostatic interactions to the observed partitioning of the 10E8-3R Fab, we next quantified the antibody-membrane interaction by spectroscopic titration of NBD-labeled Fab against vesicles that combined DOPC and DOPS lipids at

different molar ratios (40, 41) (Fig. 4). The experimental values, adjusted to Equation [1], allowed estimation of a mole-fraction partition coefficient ($K_x$) of 0.2 x $10^7$ for DOPC:DOPS (50:50) vesicles, a value that falls in the range of that observed for peripheral membrane proteins such as the Phospholipase C-ζ or the juxtamembrane domain of ErbB1 (42, 43). Moreover, the $K_x$ values decreased upon reduction of the content of the negatively charged lipid DOPS (Fig. 4A). Consistently, the linear plot of partitioning free energies ($\Delta G_{obs}$) as a function of the surface potential ($\Psi_0$) displayed positive slope (Fig. 4B), following the pattern expected for antibody-membrane interactions being driven by electrostatic forces (35, 44). In conclusion, 10E8-3R followed a membrane-binding mechanism that resembled a peripheral membrane interaction, as has been described previously for the Fab 4E10 (reference (25); see also below).

*Effects imparted by the 3R mutation on the biological function of 10E8*

Having determined that the 3R mutations enabled 10E8 binding to lipid vesicles, we tested their effect on polyreactivity and neutralizing activity (Figs. 5 and 6). We assessed first the propensity of 10E8 and cognate 3R mutant to bind to HEp-2 cells, which have been used previously for determining antibody polyreactivity (8, 45). We found that, in contrast to the positive control, 4E10 IgG, neither 10E8-WT nor 10E8-3R bound to HEp-2 epithelial cells (Fig. 5A). We also compared the polyreactivity of 10E8-WT and 10E8-3R in a standard ELISA (8, 46) against various lipids, DNAs, as well as unrelated proteins, ovalbumin (OVA) and BSA. By these assays, neither 10E8-WT nor 10E8-3R showed significant polyreactivity

366 even at high concentration, with the exception of POPC binding, in which case 10E8 and the
367 3R mutant showed similarly weak binding signals as the 4E10 IgG control (Fig. 5B).

368 We next tested the effect of the 3R mutations on the neutralization capacity of 10E8 against
369 a panel of six HIV-1 isolates used previously as an indicator of cross-clade neutralization
370 breadth (47). As illustrated by the data displayed in Figure 6, 10E8-3R was notably more
371 potent against all six isolates relative to 10E8-WT (5- to 35-fold decrease in $IC_{50}$; Table 1).
372 An additional 10 isolates were tested in which 10E8-3R was also more potent against the
373 majority of these, including SIV strain TAN2 (Table 1). In total, the 3R mutations increased
374 10E8 neutralization potency against 14 of 16 isolates, with an average 8.9-fold decrease in
375 $IC_{50}$; however, neutralization potency did not change against two isolates (Q23.17 and
376 CH181.12), so the effect appears to be somewhat isolate dependent.

377

378 *10E8-3R antibody engagement with MPER peptide and HIV-1 Env*

379 That the 3R mutation did not make 10E8 polyreactive indicates that the differences in binding
380 and neutralization of 10E8 caused by the mutations are specific. It has been shown that 10E8
381 neutralizing activity correlates with its capacity for epitope recognition in a membrane
382 environment (3). Therefore, we sought to establish whether the overall enhanced
383 neutralization observed for 10E8-3R correlated with an improved epitope binding function
384 (Figs. 7 and 8).

385 Top panels in Figure 7A display confocal images of peptide-containing GUVs that were
386 probed by Laurdan label and with the KK114-10E8-WT Fab. These GUVs exhibited
387 simultaneous staining of the lipid bilayer by both Laurdan and KK114 probes (green and red

colors, respectively), consistent with previously reported binding of 10E8 to MPER peptide inserted into membranes (3). The relatively intense KK114 staining of GUVs observed upon incubation with Fab KK114-10E8-3R suggests that the optimized 3R mutant bound with a higher apparent affinity than parental antibody to GUV membranes decorated with epitope-peptide (Fig. 7A, bottom panels). These observations were further supported by experiments performed using NBD-labeled Fabs (Figs. 7B,C). Binding to vesicles containing MPER peptide resulted in NBD fluorescence changes (Fig. 7B), i.e., increase in emission and maximum blue-shift (Fig. 7C), that were overall more prominent in the 10E8-3R variant than in the parental Fab 10E8-WT. This observation was again consistent with more efficient epitope recognition in the membrane milieu by the 3R mutant.

To determine whether the increase in neutralization by 10E8-3R corresponded to an increase in its binding affinity for virion-associated Env trimers, we next turned to a BN-PAGE gel mobility shift assay. Virions were produced from a molecular clone of Comb-mut whose Env has been shown to be >95% cleaved and trimeric (39). When a Fab binds to the Env spike the trimer will run more slowly on BN-PAGE, shifting the cognate band upwards on the gel. 10E8-3R Fab shifted the trimer band at a 5-fold lower concentration than 10E8-WT suggesting that the 3R mutations increased affinity for the trimer (Figs. 8A and C; shifting $EC_{50}$s of 2.3 μg/ml for WT, and 0.47 μg/ml for 3R). To query whether the membrane contributed to the enhanced binding capacity of the 10E8-3R Fab we also performed a "washout" version of the gel mobility shift assay, in which virus was pelleted and unbound antibody was removed prior to adding detergent. This experiment yielded similar results as the standard assay (Figs. 8B and C). We conclude that the 3R mutations enhance 10E8 binding to the unliganded Env trimer in the virus membrane. We note that neutralization by

411 10E8 and other MPER antibodies typically involves binding to both unliganded Env and
412 receptor-activated forms of Env, and it is possible that the 3R mutations also affect binding
413 to the latter state of Env but this was not tested here due to the experimental challenges
414 involved.

415

416

417 *Effects imparted by a 3R mutation on 4E10*

418 Given the potential implications for ongoing efforts in vaccine and biologics design, our
419 optimization approach focused primarily on the highly potent antibody 10E8. To establish
420 whether the same strategy to improve neutralization efficacy by strengthening electrostatic
421 interactions with membranes could be applied to other anti-MPER antibodies, we introduced
422 three Arg mutations into the paratope of the 4E10 antibody (Fig. 9 and Table 2). The first-
423 generation anti-MPER bnAb 4E10 has already been shown to spontaneously partition into
424 membranes (24, 25), exhibits some polyreactivity, particularly with lipids, and is less potent
425 than 10E8 (see reference (8) for a side-by-side comparison of both antibodies).

426 Thus, to generate the 4E10-3R mutant we introduced the triple substitution
427 G27R/S30R/S74R to the heavy chain of the Fab 4E10, which resulted in an increased positive
428 charge at the flat paratope surface predicted by crystallography to contact the interface of the
429 lipid bilayer (22) (Figs. 9A, B). These changes did not affect binding to epitope peptide in
430 ELISA (not shown). However, the Fab 4E10-3R partitioned more effectively into vesicles
431 than the parental 4E10-WT (Fig. 9C), and this effect was mediated by the establishment of
432 stronger electrostatic interactions with membranes (Fig. 9D). The 3R mutation also resulted

433 in significantly enhanced polyreactivity (Fig. 9E), but did not improve 4E10 neutralization
434 relative to 4E10-WT against any of the isolates tested, and in several cases resulted in up to
435 a 2-fold increase in $IC_{50}$ (Table 2). Moreover, in line with the lack of neutralization
436 improvement, the WT and 3R mutant Fabs shifted to similar extents the mobility of the Env
437 trimer in BN-PAGE experiments (Fig. 9F).

438 In conclusion, whereas electrostatic interaction with membranes and polyreactivity were
439 enhanced with 4E10-3R relative to 4E10-WT, neutralization efficacy and Env trimer
440 engagement were less affected, or even slightly diminished. We note that while these results
441 with 4E10-3R contrast with those of 10E8-3R they do not negate the hypothesized
442 mechanism for improvement of 10E8 by 3R as those mutations are specific to 10E8, and it
443 is possible that the 4E10 3R mutations are not optimally positioned to augment the
444 neutralization potency of 4E10 by this mechanism.

445

446

447 **Discussion**

448

449 The identification of numerous highly potent bnAbs in the past decade has greatly advanced
450 our understanding of effective humoral responses elicited during HIV-1 infection (1, 11).
451 The knowledge gained has stimulated approaches for rational vaccine development (48-50).
452 The isolated bnAbs have also inspired the rational design of biologics expected to prevent

453 and treat HIV infection (51, 52). Indeed, passive administration of engineered versions of
454 bnAbs has been shown to prevent HIV infection in animal models (53, 54).

455 In this context, the potency and breadth of neutralization by 10E8 as well as its effectiveness
456 at conferring cross protection *in vivo* in primate models (8, 15-17), makes it potentially useful
457 for therapeutic developments. Two complementary strategies have been followed to
458 overcome potential limitations of 10E8 for pharmacological use, namely: i) optimization of
459 function and stability through mutagenesis (19), and ii) promotion of polyvalence by
460 antibody engineering (55). Following the latter strategy, recently published works describe
461 antibodies that simultaneously interact with two (bivalent) or three (trivalent) independent
462 Env determinants, which contained the paratope of 10E8 as a basic component (18, 20, 56).

463 In this work, following strategy (i) we have explored the possibility that the function of 10E8
464 can be upgraded by promoting its interaction with membranes (Fig. 1). Recent structural
465 studies define a membrane-interacting surface on the light chain of 10E8, which is juxtaposed
466 by its CDRH3 that contacts the MPER helix on Env (Fig. 1) (2-5, 22). In principle at least,
467 interaction of MPER antibodies through similar patches could be driven by coulombic
468 attraction between exposed basic residues and anionic phospholipids, a possibility that has
469 been formally demonstrated in the case of the 4E10 antibody (25). Likewise, in the case of
470 the 10E8 antibody, substitution of aspartate or glutamate at positions normally occupied by
471 basic and polar residues on the membrane-contacting patch greatly reduced neutralization
472 potency of this antibody (4).

473 Here we have asked whether manipulation of the membrane-contacting surface of 10E8 to
474 increase its net charge would enable spontaneous interaction with membranes, and what

475 effects this property might have on its biological function. We showed that the triple
476 substitution S30R/N52R/S67R in the light chain of Fab 10E8 (Fig. 1), enabled it to interact
477 spontaneously with lipid bilayers (Figs. 2-4). This change importantly also results in more
478 potent neutralizing activity (Fig. 6 and Table 1). Notably, the improvement in 10E8 function
479 correlated with enhanced binding affinity not only for the MPER epitope peptide in a
480 membrane environment (Fig. 7) but also for virion-associated Env (Fig. 8), yet had no
481 observable effect on polyreactivity, which remained almost undetectable for the 3R mutant
482 (Fig. 5). This observation implies a lack of correlation between neutralization potency and
483 polyreactivity. It further highlights a difference between partitioning from water into
484 membranes and lipid polyreactivity, as inferred from the comparison of the results in Figures
485 2-4 and 5, respectively.

486 The data obtained with the 4E10 antibody (Fig. 9) further support this concept. Upon
487 introduction of a cognate 3R mutation (Figs. 9A, B), electrostatic interactions intensified
488 resulting in stronger 4E10 association with the membrane (Figs. 9C, D), and also notably,
489 apparent polyreactivity (Fig. 9E). However, these enhancing effects neither translated into
490 better, nor worse neutralization activity (Table 2). Likewise, introduction of the 3R mutation
491 into the Fab 4E10 did not significantly affect affinity for virion-associated Env (Fig. 9F).
492 Given that 4E10 is less potent than the second-generation bnAbs (1), and, therefore, has
493 considerable scope for improving its potency, our observations argue against the postulate
494 that 4E10 polyreactivity and neutralization are contingent on each other (45, 57, 58).

495 We showed that the 3R mutations enhanced neutralization by 10E8 with most isolates, but
496 there was variation in the magnitude of the effect, and neutralization of two isolates was not
497 improved. Analysis of Env sequences of tested isolates revealed no clear signature in or near

to the MPER that would explain the strain-dependence of enhanced neutralization (our unpublished observations). However, it is possible that residues surrounding the MPER alter the effect of the 3R mutations on neutralization. Alternatively, the differential effect of 3R on neutralization between isolates could relate to differences in kinetics of fusion, proximal glycosylation or MPER conformation relative to the antibody in different Env backgrounds. Further studies of Env structure and mechanisms of 10E8 recognition are necessary to address these issues.

Thus, although our data support the idea that interactions with the viral membrane surface occur during the neutralization mechanism of anti-MPER antibodies, they caution that the proposed two-step model in which anti-MPER antibodies first attach to the viral membrane and then to the Env antigen (59-61) might be of limited applicability. The finding that enhanced membrane interaction does not affect 4E10 neutralization potency implies that accumulation of this antibody at the virus membrane does not necessarily play a role in the mechanism of neutralization. That the Fab 10E8, which is more potent than 4E10, does not spontaneously interact with VL membranes (Figs. 2 and 3) also goes against the assumption that pre-attachment of this antibody to the viral membrane is strictly required during neutralization (61).

Our data rather indicate that antibody-membrane interactions might function at a step after- or concomitant with- the engagement of the Env antigen. Membrane binding thus would stabilize the antibody-Env complex resulting in a high-affinity interaction and higher neutralization potency, at least in the case of 10E8 (Figs. 6-8). That there is some Env dependence to the magnitude of this effect, suggests that elements in Env may influence accessibility to the membrane interacting region, as in a specific bipartite Env-membrane

epitope, rather than independent membrane and Env binding sites of a simple two-step model. Since reducing electrostatic interactions with membranes hinders 4E10-induced neutralization (25), but their enhancement has no effect (Fig. 9 and Table 2), it seems possible that the contribution of electrostatic antibody-membrane interactions to the mechanism of 4E10 neutralization has already reached an optimal level. Alternatively, the membrane-contacting surface relevant to 4E10 neutralization might be different to that inferred from prior crystal structures and mutagenesis studies (22, 25). Thus, it cannot be excluded that the 3R residues have been incorporated at irrelevant positions on 4E10. On the other hand, the available structures for 10E8 may reflect more precisely its functional binding state.

In conclusion, our observations suggest that electrostatic interactions between anti-MPER antibodies and the lipid bilayer result from structural adaptations to enable functional binding to Env in the membrane milieu (2-4, 22, 24, 25). If this idea is correct, we infer that vaccines targeting the MPER epitope should elicit antibodies that approximate if not reproduce cognate membrane interactions. Our data also demonstrate that with 10E8 there is scope for functional improvement by engineering the membrane-interacting surface of the paratope, a strategy that should be further explored.

**Acknowledgements.**

This study was supported by the Spanish MINECO (BIO2015-64421-R (MINECO/FEDER UE) to JLN) and the Basque Government (IT838-13 to JLN). Support was also provided by the NIH NIAID (R01 AI114401 and R01 AI098602 to MBZ) and from the James B.

Pendleton Charitable Trust (MBZ). ER and SI received pre-doctoral fellowships from the Basque Government. We acknowledge valuable technical assistance from Dr. Rubén Sanchez-Eugenia and Miguel García-Porras.

**References:**


1. **Burton DR, Hangartner L.** 2016. Broadly Neutralizing Antibodies to HIV and Their Role in Vaccine Design. Annu Rev Immunol **34:**635-659.

2. **Lee JH, Ozorowski G, Ward AB.** 2016. Cryo-EM structure of a native, fully glycosylated, cleaved HIV-1 envelope trimer. Science **351:**1043-1048.

3. **Rujas E, Caaveiro JM, Partida-Hanon A, Gulzar N, Morante K, Apellaniz B, Garcia-Porras M, Bruix M, Tsumoto K, Scott JK, Jimenez MA, Nieva JL.** 2016. Structural basis for broad neutralization of HIV-1 through the molecular recognition of 10E8 helical epitope at the membrane interface. Sci Rep **6:**38177.

4. **Irimia A, Serra AM, Sarkar A, Jacak R, Kalyuzhniy O, Sok D, Saye-Francisco KL, Schiffner T, Tingle R, Kubitz M, Adachi Y, Stanfield RL, Deller MC, Burton DR, Schief WR, Wilson IA.** 2017. Lipid interactions and angle of approach to the HIV-1 viral membrane of broadly neutralizing antibody 10E8: Insights for vaccine and therapeutic design. PLoS Pathog **13:**e1006212.

5. **Cerutti N, Loredo-Varela JL, Caillat C, Weissenhorn W.** 2017. Antigp41 membrane proximal external region antibodies and the art of using the membrane for neutralization. Curr Opin HIV AIDS **12:**250-256.

6. **Zwick MB, Labrijn AF, Wang M, Spenlehauer C, Saphire EO, Binley JM, Moore JP, Stiegler G, Katinger H, Burton DR, Parren PW.** 2001. Broadly neutralizing antibodies targeted to the membrane-proximal external region of human immunodeficiency virus type 1 glycoprotein gp41. J Virol **75:**10892-10905.

7. **Binley JM, Wrin T, Korber B, Zwick MB, Wang M, Chappey C, Stiegler G, Kunert R, Zolla-Pazner S, Katinger H, Petropoulos CJ, Burton DR.** 2004. Comprehensive cross-clade neutralization analysis of a panel of anti-human immunodeficiency virus type 1 monoclonal antibodies. J Virol **78:**13232-13252.

8. **Huang J, Ofek G, Laub L, Louder MK, Doria-Rose NA, Longo NS, Imamichi H, Bailer RT, Chakrabarti B, Sharma SK, Alam SM, Wang T, Yang Y, Zhang**

**B, Migueles SA, Wyatt R, Haynes BF, Kwong PD, Mascola JR, Connors M.** 2012. Broad and potent neutralization of HIV-1 by a gp41-specific human antibody. Nature **491:**406-412.

9. **Jacob RA, Moyo T, Schomaker M, Abrahams F, Grau Pujol B, Dorfman JR.** 2015. Anti-V3/Glycan and Anti-MPER Neutralizing Antibodies, but Not Anti-V2/Glycan Site Antibodies, Are Strongly Associated with Greater Anti-HIV-1 Neutralization Breadth and Potency. J Virol **89:**5264-5275.

10. **Kim AS, Leaman DP, Zwick MB.** 2014. Antibody to gp41 MPER alters functional properties of HIV-1 Env without complete neutralization. PLoS Pathog **10:**e1004271.

11. **Kwong PD, Mascola JR.** 2012. Human antibodies that neutralize HIV-1: identification, structures, and B cell ontogenies. Immunity **37:**412-425.

12. **Zwick MB.** 2005. The membrane-proximal external region of HIV-1 gp41: a vaccine target worth exploring. Aids **19:**1725-1737.

13. **Montero M, van Houten NE, Wang X, Scott JK.** 2008. The membrane-proximal external region of the human immunodeficiency virus type 1 envelope: dominant site of antibody neutralization and target for vaccine design. Microbiol Mol Biol Rev **72:**54-84, table of contents.

14. **Burton DR, Mascola JR.** 2015. Antibody responses to envelope glycoproteins in HIV-1 infection. Nat Immunol **16:**571-576.

15. **Pegu A, Yang ZY, Boyington JC, Wu L, Ko SY, Schmidt SD, McKee K, Kong WP, Shi W, Chen X, Todd JP, Letvin NL, Huang J, Nason MC, Hoxie JA, Kwong PD, Connors M, Rao SS, Mascola JR, Nabel GJ.** 2014. Neutralizing antibodies to HIV-1 envelope protect more effectively in vivo than those to the CD4 receptor. Sci Transl Med **6:**243ra288.

16. **van Gils MJ, Sanders RW.** 2014. In vivo protection by broadly neutralizing HIV antibodies. Trends Microbiol **22:**550-551.

17. **Barbian HJ, Decker JM, Bibollet-Ruche F, Galimidi RP, West AP, Jr., Learn GH, Parrish NF, Iyer SS, Li Y, Pace CS, Song R, Huang Y, Denny TN, Mouquet H, Martin L, Acharya P, Zhang B, Kwong PD, Mascola JR, Verrips CT, Strokappe NM, Rutten L, McCoy LE, Weiss RA, Brown CS, Jackson R, Silvestri G, Connors M, Burton DR, Shaw GM, Nussenzweig MC, Bjorkman PJ, Ho DD, Farzan M, Hahn BH.** 2015. Neutralization properties of simian immunodeficiency viruses infecting chimpanzees and gorillas. MBio **6**.

18. **Asokan M, Rudicell RS, Louder M, McKee K, O'Dell S, Stewart-Jones G, Wang K, Xu L, Chen X, Choe M, Chuang G, Georgiev IS, Joyce MG, Kirys T, Ko S, Pegu A, Shi W, Todd JP, Yang Z, Bailer RT, Rao S, Kwong PD, Nabel GJ, Mascola JR.** 2015. Bispecific Antibodies Targeting Different Epitopes on the HIV-1 Envelope Exhibit Broad and Potent Neutralization. J Virol **89:**12501-12512.

19. **Kwon YD, Georgiev IS, Ofek G, Zhang B, Asokan M, Bailer RT, Bao A, Caruso W, Chen X, Choe M, Druz A, Ko SY, Louder MK, McKee K, O'Dell S, Pegu A, Rudicell RS, Shi W, Wang K, Yang Y, Alger M, Bender MF, Carlton K, Cooper JW, Blinn J, Eudailey J, Lloyd K, Parks R, Alam SM, Haynes BF, Padte NN, Yu J, Ho DD, Huang J, Connors M, Schwartz RM, Mascola JR, Kwong PD.** 2016. Optimization of the Solubility of HIV-1-Neutralizing Antibody 10E8 through Somatic Variation and Structure-Based Design. J Virol **90:**5899-5914.

20. **Xu L, Pegu A, Rao E, Doria-Rose N, Beninga J, McKee K, Lord DM, Wei RR, Deng G, Louder M, Schmidt SD, Mankoff Z, Wu L, Asokan M, Beil C, Lange C, Leuschner WD, Kruip J, Sendak R, Do Kwon Y, Zhou T, Chen X, Bailer RT, Wang K, Choe M, Tartaglia LJ, Barouch DH, O'Dell S, Todd JP, Burton DR, Roederer M, Connors M, Koup RA, Kwong PD, Yang ZY, Mascola JR, Nabel GJ.** 2017. Trispecific broadly neutralizing HIV antibodies mediate potent SHIV protection in macaques. Science doi:10.1126/science.aan8630.

21. **Apellaniz B, Rujas E, Serrano S, Morante K, Tsumoto K, Caaveiro JM, Jimenez MA, Nieva JL.** 2015. The Atomic Structure of the HIV-1 gp41 Transmembrane Domain and Its Connection to the Immunogenic Membrane-proximal External Region. J Biol Chem **290:**12999-13015.

22. **Irimia A, Sarkar A, Stanfield RL, Wilson IA.** 2016. Crystallographic Identification of Lipid as an Integral Component of the Epitope of HIV Broadly Neutralizing Antibody 4E10. Immunity **44:**21-31.

23. **Scherer EM, Leaman DP, Zwick MB, McMichael AJ, Burton DR.** 2010. Aromatic residues at the edge of the antibody combining site facilitate viral glycoprotein recognition through membrane interactions. Proc Natl Acad Sci U S A **107:**1529-1534.

24. **Rujas E, Insausti S, Garcia-Porras M, Sanchez-Eugenia R, Tsumoto K, Nieva JL, Caaveiro JM.** 2017. Functional Contacts between MPER and the Anti-HIV-1 Broadly Neutralizing Antibody 4E10 Extend into the Core of the Membrane. J Mol Biol **429:**1213-1226.

25. **Rujas E, Caaveiro JM, Insausti S, Garcia-Porras M, Tsumoto K, Nieva JL.** 2017. Peripheral Membrane Interactions Boost the Engagement by an Anti-HIV-1 Broadly Neutralizing Antibody. J Biol Chem **292:**5571-5583.

26. **Kawai T, Caaveiro JMM, Abe R, Katagiri T, Tsumoto K.** 2011. Catalytic activity of MsbA reconstituted in nanodisc particles is modulated by remote interactions with the bilayer. FEBS Lett **585:**3533-3537.

27. **Shepard LA, Heuck AP, Hamman BD, Rossjohn J, Parker MW, Ryan KR, Johnson AE, Tweten RK.** 1998. Identification of a membrane-spanning domain of the thiol-activated pore-forming toxin Clostridium perfringens perfringolysin O: an alpha-helical to beta-sheet transition identified by fluorescence spectroscopy. Biochemistry **37:**14563-14574.

28. **Heuck AP, Hotze EM, Tweten RK, Johnson AE.** 2000. Mechanism of membrane insertion of a multimeric beta-barrel protein: perfringolysin O creates a pore using ordered and coupled conformational changes. Mol Cell **6:**1233-1242.

29. **Hope MJ, Bally MB, Webb G, Cullis PR.** 1985. Production of large unilamellar vesicles by a rapid extrusion procedure. Characterization of size distribution, trapped volume and ability to maintain a membrane potential. Biochim Biophys Acta **812:**55-65.

30. **Mattila J-P, Shnyrova AV, Sundborger AC, Hortelano ER, Fuhrmans M, Neumann S, Muller M, Hinshaw JE, Schmid SL, Frolov VA.** 2015. A hemi-fission intermediate links two mechanistically distinct stages of membrane fission. Nature **524:**109-113.

31. **Carravilla P, Nieva JL, Goñi FM, Requejo-Isidro J, Huarte N.** 2015. Two-Photon Laurdan Studies of the Ternary Lipid Mixture DOPC:SM:Cholesterol Reveal a Single Liquid Phase at Sphingomyelin:Cholesterol Ratios Lower Than 1. Langmuir **31:**2808-2817.

32. **Yethon JA, Epand RF, Leber B, Epand RM, Andrews DW.** 2003. Interaction with a membrane surface triggers a reversible conformational change in Bax normally associated with induction of apoptosis. J Biol Chem **278:**48935-48941.

33. **Huarte N, Carravilla P, Cruz A, Lorizate M, Nieto-Garai JA, Krausslich HG, Perez-Gil J, Requejo-Isidro J, Nieva JL.** 2016. Functional organization of the HIV lipid envelope. Sci Rep **6:**34190.

34. **White SH, Wimley WC, Ladokhin AS, Hristova K.** 1998. Protein folding in membranes: Determining energetics of peptide-bilayer interactions, p 62-87, Methods in Enzymology, vol Volume 295. Academic Press.

35. **McLaughlin S.** 1989. The electrostatic properties of membranes. Annu Rev Biophys Biophys Chem **18:**113-136.

36. **Rand RP, Parsegian VA.** 1989. Hydration forces between phospholipid bilayers. Biochim Biophys Acta **988:**351-376.

37. **Wei X, Decker JM, Wang S, Hui H, Kappes JC, Wu X, Salazar-Gonzalez JF, Salazar MG, Kilby JM, Saag MS, Komarova NL, Nowak MA, Hahn BH, Kwong PD, Shaw GM.** 2003. Antibody neutralization and escape by HIV-1. Nature **422:**307-312.

38. **Leaman DP, Kinkead H, Zwick MB.** 2010. In-solution virus capture assay helps deconstruct heterogeneous antibody recognition of human immunodeficiency virus type 1. J Virol **84:**3382-3395.

39. **Leaman DP, Zwick MB.** 2013. Increased functional stability and homogeneity of viral envelope spikes through directed evolution. PLoS Pathog **9:**e1003184.

40. **Arbuzova A, Wang J, Murray D, Jacob J, Cafiso DS, McLaughlin S.** 1997. Kinetics of interaction of the myristoylated alanine-rich C kinase substrate, membranes, and calmodulin. J Biol Chem **272:**27167-27177.

41. **Arbuzova A, Wang L, Wang J, Hangyas-Mihalyne G, Murray D, Honig B, McLaughlin S.** 2000. Membrane binding of peptides containing both basic and aromatic residues. Experimental studies with peptides corresponding to the scaffolding region of caveolin and the effector region of MARCKS. Biochemistry **39:**10330-10339.

42. **Nomikos M, Mulgrew-Nesbitt A, Pallavi P, Mihalyne G, Zaitseva I, Swann K, Lai FA, Murray D, McLaughlin S.** 2007. Binding of phosphoinositide-specific phospholipase C-zeta (PLC-zeta) to phospholipid membranes: potential role of an unstructured cluster of basic residues. J Biol Chem **282:**16644-16653.

43. **McLaughlin S, Smith SO, Hayman MJ, Murray D.** 2005. An electrostatic engine model for autoinhibition and activation of the epidermal growth factor receptor (EGFR/ErbB) family. J Gen Physiol **126:**41-53.

44. **White SH, Wimley WC.** 1999. Membrane protein folding and stability: physical principles. Annu Rev Biophys Biomol Struct **28:**319-365.

45. **Haynes BF, Fleming J, St Clair EW, Katinger H, Stiegler G, Kunert R, Robinson J, Scearce RM, Plonk K, Staats HF, Ortel TL, Liao HX, Alam SM.** 2005. Cardiolipin polyspecific autoreactivity in two broadly neutralizing HIV-1 antibodies. Science **308:**1906-1908.

46. **Nelson JD, Brunel FM, Jensen R, Crooks ET, Cardoso RM, Wang M, Hessell A, Wilson IA, Binley JM, Dawson PE, Burton DR, Zwick MB.** 2007. An affinity-enhanced neutralizing antibody against the membrane-proximal external region of human immunodeficiency virus type 1 gp41 recognizes an epitope between those of 2F5 and 4E10. J Virol **81:**4033-4043.

47. **Simek MD, Rida W, Priddy FH, Pung P, Carrow E, Laufer DS, Lehrman JK, Boaz M, Tarragona-Fiol T, Miiro G, Birungi J, Pozniak A, McPhee DA, Manigart O, Karita E, Inwoley A, Jaoko W, Dehovitz J, Bekker LG, Pitisuttithum P, Paris R, Walker LM, Poignard P, Wrin T, Fast PE, Burton DR, Koff WC.** 2009. Human immunodeficiency virus type 1 elite neutralizers: individuals with broad and potent neutralizing activity identified by using a high-throughput neutralization assay together with an analytical selection algorithm. J Virol **83:**7337-7348.

48. **Haynes BF, Mascola JR.** 2017. The quest for an antibody-based HIV vaccine. Immunol Rev **275:**5-10.

49. **Kwong PD.** 2017. What Are the Most Powerful Immunogen Design Vaccine Strategies? A Structural Biologist's Perspective. Cold Spring Harb Perspect Biol doi:10.1101/cshperspect.a029470.

50. **Burton DR.** 2017. What Are the Most Powerful Immunogen Design Vaccine Strategies? Reverse Vaccinology 2.0 Shows Great Promise. Cold Spring Harb Perspect Biol doi:10.1101/cshperspect.a030262.

51. **Klein F, Mouquet H, Dosenovic P, Scheid JF, Scharf L, Nussenzweig MC.** 2013. Antibodies in HIV-1 vaccine development and therapy. Science **341:**1199-1204.

52. **West AP, Jr., Scharf L, Scheid JF, Klein F, Bjorkman PJ, Nussenzweig MC.** 2014. Structural insights on the role of antibodies in HIV-1 vaccine and therapy. Cell **156:**633-648.

53. **Barouch DH, Whitney JB, Moldt B, Klein F, Oliveira TY, Liu J, Stephenson KE, Chang HW, Shekhar K, Gupta S, Nkolola JP, Seaman MS, Smith KM, Borducchi EN, Cabral C, Smith JY, Blackmore S, Sanisetty S, Perry JR, Beck M, Lewis MG, Rinaldi W, Chakraborty AK, Poignard P, Nussenzweig MC, Burton DR.** 2013. Therapeutic efficacy of potent neutralizing HIV-1-specific monoclonal antibodies in SHIV-infected rhesus monkeys. Nature **503:**224-228.

54. **Halper-Stromberg A, Lu CL, Klein F, Horwitz JA, Bournazos S, Nogueira L, Eisenreich TR, Liu C, Gazumyan A, Schaefer U, Furze RC, Seaman MS, Prinjha R, Tarakhovsky A, Ravetch JV, Nussenzweig MC.** 2014. Broadly Neutralizing Antibodies and Viral Inducers Decrease Rebound from HIV-1 Latent Reservoirs in Humanized Mice. Cell **158:**989-999.

55. **Montefiori DC.** 2016. Bispecific Antibodies Against HIV. Cell **165:**1563-1564.

56. **Huang Y, Yu J, Lanzi A, Yao X, Andrews CD, Tsai L, Gajjar MR, Sun M, Seaman MS, Padte NN, Ho DD.** 2016. Engineered Bispecific Antibodies with Exquisite HIV-1-Neutralizing Activity. Cell **165:**1621-1631.

57. **Verkoczy L, Kelsoe G, Haynes BF.** 2014. HIV-1 envelope gp41 broadly neutralizing antibodies: hurdles for vaccine development. PLoS Pathog **10:**e1004073.

58. **Finton KA, Larimore K, Larman HB, Friend D, Correnti C, Rupert PB, Elledge SJ, Greenberg PD, Strong RK.** 2013. Autoreactivity and exceptional CDR plasticity (but not unusual polyspecificity) hinder elicitation of the anti-HIV antibody 4E10. PLoS Pathog **9:**e1003639.

59. **Alam SM, Morelli M, Dennison SM, Liao HX, Zhang R, Xia SM, Rits-Volloch S, Sun L, Harrison SC, Haynes BF, Chen B.** 2009. Role of HIV membrane in neutralization by two broadly neutralizing antibodies. Proc Natl Acad Sci U S A **106:**20234-20239.

60. **Haynes BF, Nicely NI, Alam SM.** 2010. HIV-1 autoreactive antibodies: are they good or bad for HIV-1 prevention? Nat Struct Mol Biol **17:**543-545.

764 61. **Chen J, Frey G, Peng H, Rits-Volloch S, Garrity J, Seaman MS, Chen B.** 2014.
765 Mechanism of HIV-1 neutralization by antibodies targeting a membrane-proximal
766 region of gp41. J Virol **88:**1249-1258.

767

768

769 **Figure Legends:**

770

771 **Figure 1: Design of 10E8 mutant with 3 Arg residues exposed on the paratope**. (A)
772 Surface density charge representation of wild-type Fab 10E8 (PDB entry code: 5GHW) and
773 its triple mutant 10E8-3R (bottom views). Negative and positive surface electrostatic
774 potentials are colored in red and blue, respectively. The triple substitution S30R/N52R/S67R
775 was introduced in the light chain (LC). Encircled patches are predicted to establish contact
776 with the membrane interface upon engagement with MPER epitope (3, 4). (B) Position of the
777 3R mutation relative to Env trimer and membrane. Left: model for the binding of Fab 10E8
778 (ribbon representation) to an Env trimer (EMDB code: EMD-3308, orange silhouette). Light
779 and heavy chains of the Fab are depicted in brown and tan colors, respectively. Right: close-
780 up view of the mutated positions (Arg side-chains in blue) on 10E8. The dotted line indicates
781 the approximate level of the membrane interface. Side-chain of W100b$_{HC}$ marks the position
782 of the CDRH3 tip inserted into the membrane (3). Modeled into the structures are a
783 phospholipid molecule 06:0 PG (PDB entry code: 5T85; colored by atoms) and the epitope
784 peptide MPER(664-690) (PDB entry code: 5GHW; orange helix). (C) Fab binding to epitope
785 peptide MPER(671-693) in ELISA (black line). The red dotted line corresponds to the signal
786 obtained for antibody binding to a control epitope peptide that contains the crucial residues
787 $^{672}$WF$^{673}$ substituted by Ala.

788

789 **Figure 2: Partitioning of Fabs into membranes measured by the vesicle flotation assay**.
790 (A) Diagram to illustrate the method. The Fabs (1.5 μM) were incubated with Rho-PE-

791 labeled VL LUVs (1.5 mM), and subsequently deposited on a stepwise sucrose gradient ($t_0$).
792 After ultracentrifugation ($t_1$), four different fractions were collected based on their densities.
793 (B) Partitioning of Fab 10E8 and its derivatives into VL LUVs. The presence of vesicles and
794 Fab in the different fractions was probed by Rho emission and Western blot, respectively.
795 VL LUVs (emission spectra at the bottom of the right panel) were found in the third and
796 fourth fractions (i.e., floated fractions). An additional fraction employing SDS was collected
797 to recover the material attached to the surface of the tube. Analyzed samples include (from
798 top to bottom): PG9, an anti-gp120 antibody used as negative control; 10E8-WT; 10E8-3R;
799 10E8-3R(-LUVs), a 10E8-R3 sample centrifuged in the absence of VL vesicles; and 10E8-
800 3R(C), a control Fab containing a 3R mutation within the constant domain. The values
801 displayed on the right correspond to the percentages of antibody found co-floating with
802 vesicles, calculated by densitometry.

803

804 **Figure 3. Partitioning into membranes measured by fluorescence techniques.** (A)
805 Partitioning of fluorescently labeled Fabs KK114-10E8-WT and KK114-10E8-3R into VL
806 GUVs. Micrographs display confocal images of VL GUVs at the equatorial plane. The lipid
807 bilayer was labeled with Laurdan, and bound antibody imaged following fluorescence
808 emission of KK114 (green and red colors, respectively). The micrographs of both samples
809 were rendered with equal contrast and brightness to best appreciate the difference in emission
810 intensity. Scale bars: 2.5 μm. (B) Diagram illustrating the spectroscopic changes, namely,
811 emission intensity increase and maximum shift, that occur after transferring from solvent to
812 membrane the fluorophore 7-nitrobenz-2-oxa-1,3-diazol-4-yl (NBD) covalently attached to
813 the CDRH3 tip of Fabs (3, 24, 25). (B) Binding of Fab 10E8 to VL LUVs monitored by

changes in NBD fluorescence. Emission spectra of NBD-10E8-WT and NBD-10E8-3R measured in solution (gray solid line) or in the presence of increasing concentrations of VL vesicles (black solid and dotted lines). Prior to spectra collection NBD-Fabs (0.5 μM) were incubated with different concentrations of VL LUVs as indicated in the panels.

**Figure 4. Binding of 10E8-3R to PC:PS LUVs monitored by changes in NBD fluorescence.** (A) Titration curves obtained by plotting the fraction of NBD-10E8-3R bound as a function of the concentration of lipid accessible on DOPC:DOPS vesicles (half the total lipid concentration) that contained 50, 25 or 10 mole % of DOPS (data depicted in blue, red and green, respectively). Each symbol on the plot represents an average of three independent experiments (±S.D. if larger than symbol). The molar fraction partition coefficients, $K_x$, displayed in the panel were calculated from the best fit of Equation [1] to the data (curves). (B) Plot of the free energy of partitioning versus the membrane-surface potential in the previous lipid vesicles, estimated according to Equations [2] and [3], respectively. The positive slope of the linear regression is consistent with the favorable contribution of electrostatic interactions to membrane partitioning.

**Figure 5. Analysis of 10E8-3R polyreactivity**. (A) Immunofluorescence staining experiment #1 using 10E8-3R against HEp-2 cells. 10E8-WT and 10E8-3R Fabs were used at a concentration of 25 μg/ml. 4E10 IgG was used as positive control. Images shown are at 200X magnification. (B) ELISA binding of 10E8-3R against various antigens. PV04 Fab and 4E10 IgG were used as a negative control and positive control, respectively.

836

837 **Figure 6. Neutralization of HIV-1 by 10E8-3R.** 10E8-WT and 10E8-3R Fabs were tested
838 in a neutralization assay using TZM-bl target cells and a cross-clade panel of HIV-1 isolates:
839 (A) 94UG103, (B) 92RW020, (C) 92BR020, (D) IAVI C22, (E) 16055, and (F) 92TH021.

840

841 **Figure 7. Effect of enhanced electrostatic interactions on epitope recognition at the**
842 **membrane surface.** (A) Partitioning of KK114-labeled Fabs 10E8-WT and 10E8-3R into
843 VL GUVs decorated with epitope peptide MPER(671-693). Conditions otherwise as in
844 previous Fig. 3. (B) Changes of fluorescence emission spectra upon incubation of NBD-
845 labeled 10E8-WT or 10E8-3R with vesicles that contained 1.7 μM of MPER(671-693) (black
846 and blue lines, respectively). The gray line represents the emission spectra of the NBD-Fabs
847 in solution. (C) Increase in fractional emission and change in the position of the maximum
848 of fluorescence emission wavelength in the presence of increasing concentrations of vesicles
849 that contained 1.7 μM peptide (top and bottom panels, respectively). The initial value of
850 fluorescence ($F_0$) was determined from the maximum intensity of the labeled Fab in solution,
851 i.e., before addition of peptide-containing vesicles. Final fluorescence values (F) correspond
852 to the NBD intensity measured after incubation with vesicles. Black and blue symbols
853 correspond to WT and 3R Fabs, respectively. Each data point corresponds to the average of
854 three titrations (± SD) as the ones displayed in the panel B.

855

856 **Figure 8. Binding of the Fab 10E8-3R to native Env trimers on virions. (**A) HIV-1 virions
857 displaying Comb-mut Env were incubated with 10E8-WT or 10E8-3R Fabs, followed by

858 treatment with mild detergent and resolution of Env-Fab complexes using BN-PAGE
859 Western blot. Binding of an antibody to the Env trimer causes it to run more slowly on the
860 gel and the cognate band to shift upwards on the blot. Estimation of the migration of a trimer
861 with one, two, or three Fabs bound (left side) is based on gel mobility shifts by control Fabs
862 PGT126 (3 Fabs/trimer), PGT151 (2 Fabs), and PG9 (1 Fab). (B) BN-PAGE gel mobility
863 shift was performed as in panel A, except that after Fabs and virus were incubated together
864 for 30 min the virus was pelleted and unbound Fab was removed. Thus, the gel mobility shift
865 only reflects binding to the trimer while it was incorporated in the virion membrane. (C) The
866 intensity of bands on BN-PAGE Western blots were quantified using ImageJ software, and
867 the percentage of the trimer bound by antibody was calculated by comparing the intensity of
868 the unliganded trimer band in the presence and absence of Fab. The results shown are the
869 average of four (standard assay) and two (washout) independent BN-PAGE Western blots.

870

871 **Figure 9: Design, membrane binding and polyreactivity of the 4E10-3R antibody.** (A)
872 Surface density charge representation (bottom views) of Fabs 4E10-WT (PDB entry code:
873 2FX7) and mutant 4E10-3R (rendered by introduction of the triple substitution
874 G27R/S30R/S74R in the heavy chain). (B) Model for interaction with an Env trimer and
875 detailed view of the mutated positions (in blue) relative to membrane (dotted line). Bound
876 phospholipid molecules (06:0 PA, colored by atoms) and MPER helix (in orange) were
877 obtained from structures with PDB entries 4XBG and 5GHW, respectively. The light and
878 heavy chain of the Fabs are shown in brown and tan colors, respectively (C) Binding of 4E10-
879 3R (blue traces and symbols) to DOPC:DOPS (50:50) LUVs monitored by changes in NBD
880 fluorescence. The black dotted line follows binding of 4E10-WT. The fraction of Fab bound

as a function of the concentration of lipid accessible (half the total lipid concentration) was plotted after titration of NBD-labeled Fab with increasing concentrations of liposomes. Conditions are otherwise as in Figure 4. (D) Plots of the free energy of partitioning versus the membrane-surface potential in the previous lipid vesicles. The black dotted line adjusts to 4E10-WT data, and is included for comparison. (E) Immunofluorescence staining experiment #2 using 4E10-3R against HEp-2 cells. 4E10-WT and 3R mutant Fabs were used at a concentration of 25 μg/ml. Images shown are at 200X magnification. (F) Binding of the Fab 4E10-3R to native Env trimers on virions. Top: HIV-1 virions displaying Comb-mut Env were incubated with 4E10-WT or 4E10-3R Fabs, and Env-Fab complexes resolved using BN-PAGE Western blot. Bottom: percentage of the trimer bound by antibody was calculated by comparing the intensity of the unliganded trimer band in the presence and absence of Fab. Conditions otherwise described in the caption for Figure 8.

## Tables

**Table 1.**

Neutralization of HIV-1 by 10E8-WT and 3R variant.

| | | | 10E8 IC50 (µg/ml) | | |
|---|---|---|---|---|---|
| **Virus** | **Clade** | **Tier** | **WT** | **3R** | **Fold Change*** |
| 92RW020 | A | 2 | 0.53 | 0.038 | 13.9 |
| 94UG103 | A | 2 | 0.46 | 0.094 | 4.9 |
| BG505 | A | 2 | 0.36 | 0.18 | 2.0 |
| Q23.17 | A | 1b | 0.024 | 0.027 | 0.9 |
| 92BR020 | B | 2 | 0.18 | 0.014 | 13.5 |
| Comb-mut | B | 2 | 0.033 | 0.0039 | 8.4 |
| JRFL | B | 2 | 0.058 | 0.013 | 4.5 |
| LAI | B | 1b | 0.090 | 0.012 | 7.5 |
| SF162 | B | 1a | 0.051 | 0.021 | 2.4 |
| 16055 | C | 2 | 0.30 | 0.016 | 18.4 |
| COT6 | C | 2 | 0.0063 | 0.0037 | 1.7 |
| Du422.01 | C | 2 | 0.040 | 0.010 | 4.0 |
| IAVI C22 | C | 2 | 0.035 | 0.0027 | 13.1 |
| CH181.12 | BC | 2 | 0.48 | 0.603 | 0.8 |
| 92TH021 | AE | 2 | 0.025 | 0.0007 | 34.9 |
| TAN2 | SIVcpz | 2 | 0.092 | 0.0078 | 11.9 |
| **Average** | | | | | **8.9** |

*Fold decrease in IC50 (WT IC50/3R IC50).

**Table 2.**

Neutralization of HIV-1 by 4E10-WT and 3R variant.

| Virus | Clade | Tier | 4E10 IC50 (µg/ml) | | Fold Change* |
|---|---|---|---|---|---|
| | | | WT | 3R | |
| BG505 | A | 2 | 1.3 | 1.4 | 0.91 |
| Comb-mut | B | 2 | 1.6 | 2.9 | 0.57 |
| SF162 | B | 1a | 1.9 | 4.6 | 0.40 |
| COT6 | C | 2 | 0.8 | 2.1 | 0.37 |
| Du422.01 | C | 2 | 0.94 | 1.00 | 0.94 |
| CH181.12 | BC | 2 | 5.4 | 10.1 | 0.53 |
| **Average** | | | | | **0.6** |

*Fold decrease in IC50 (WT IC50/3R IC50).

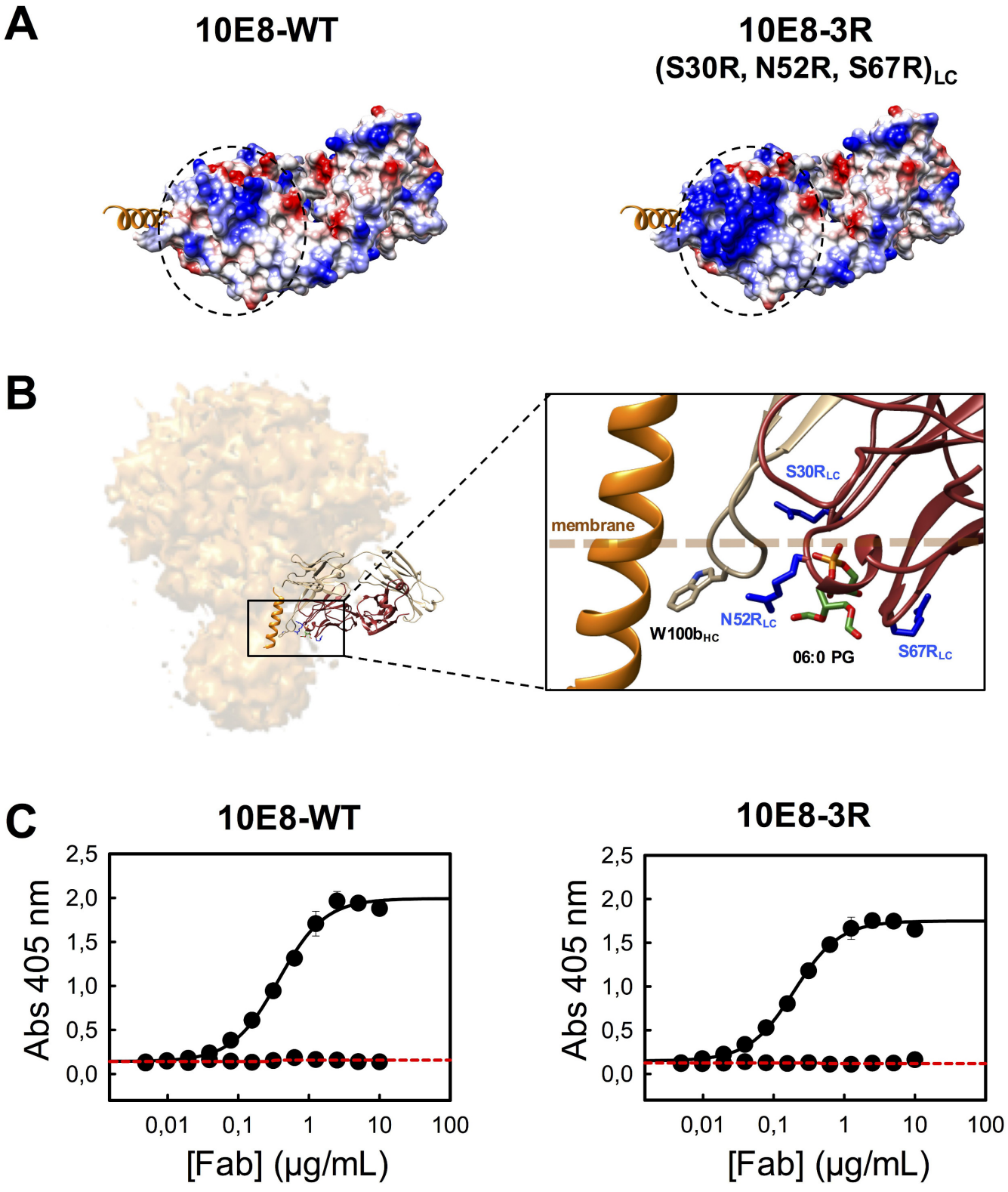

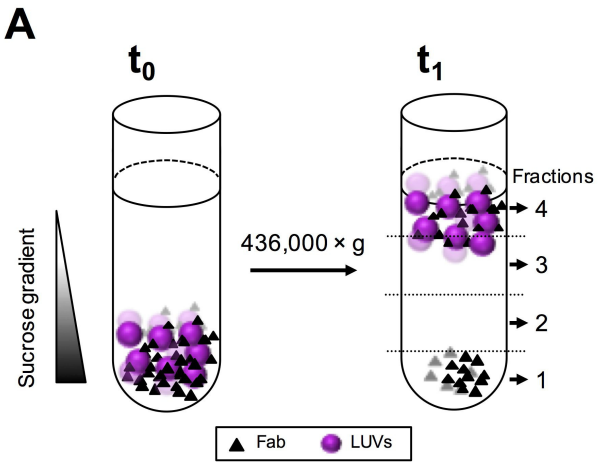


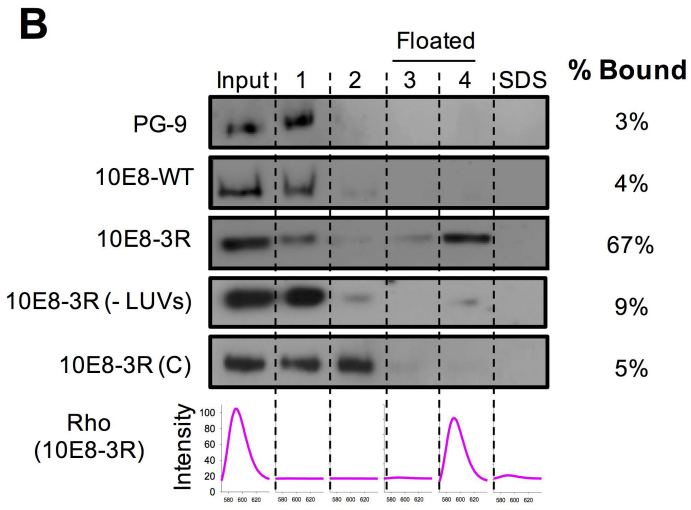

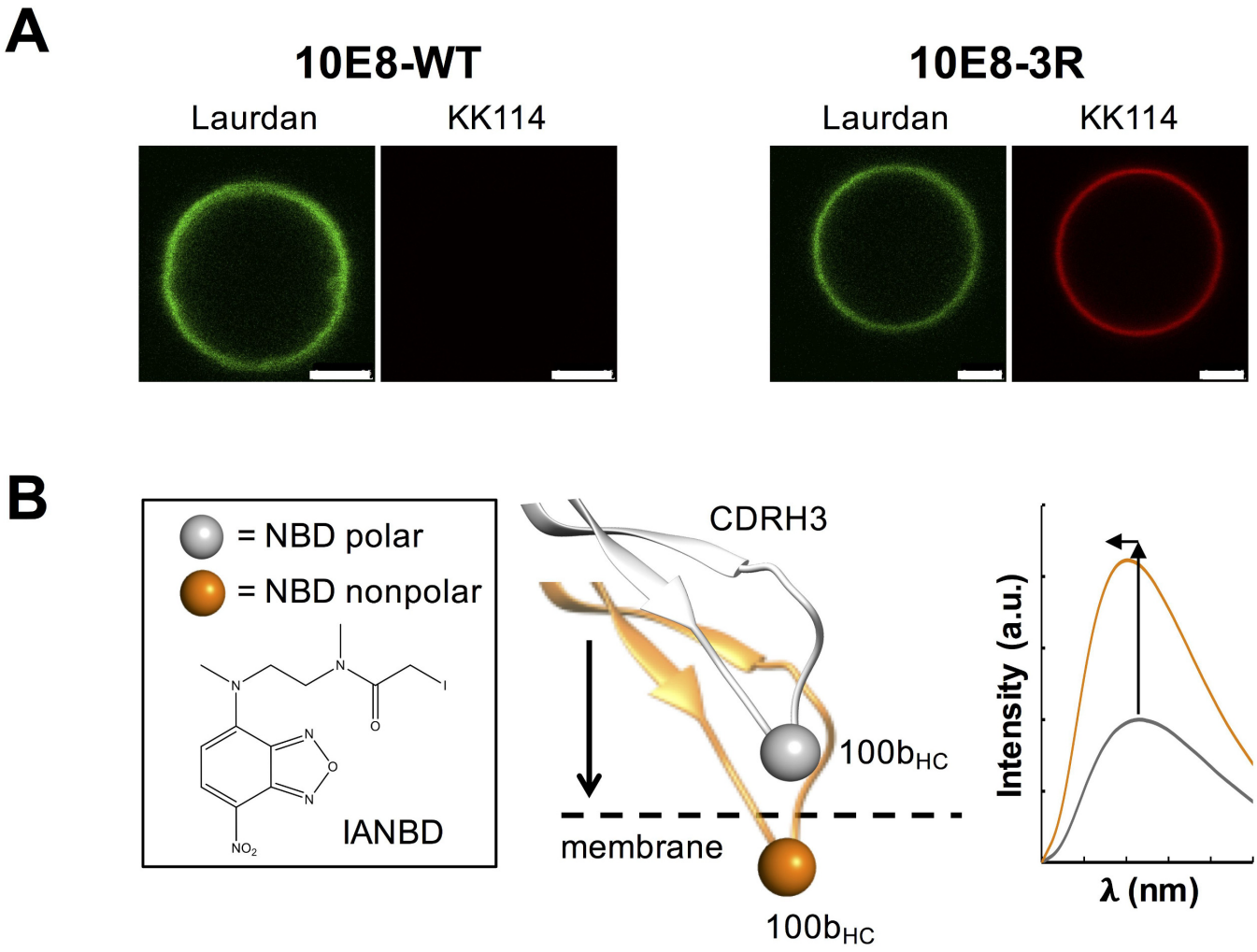

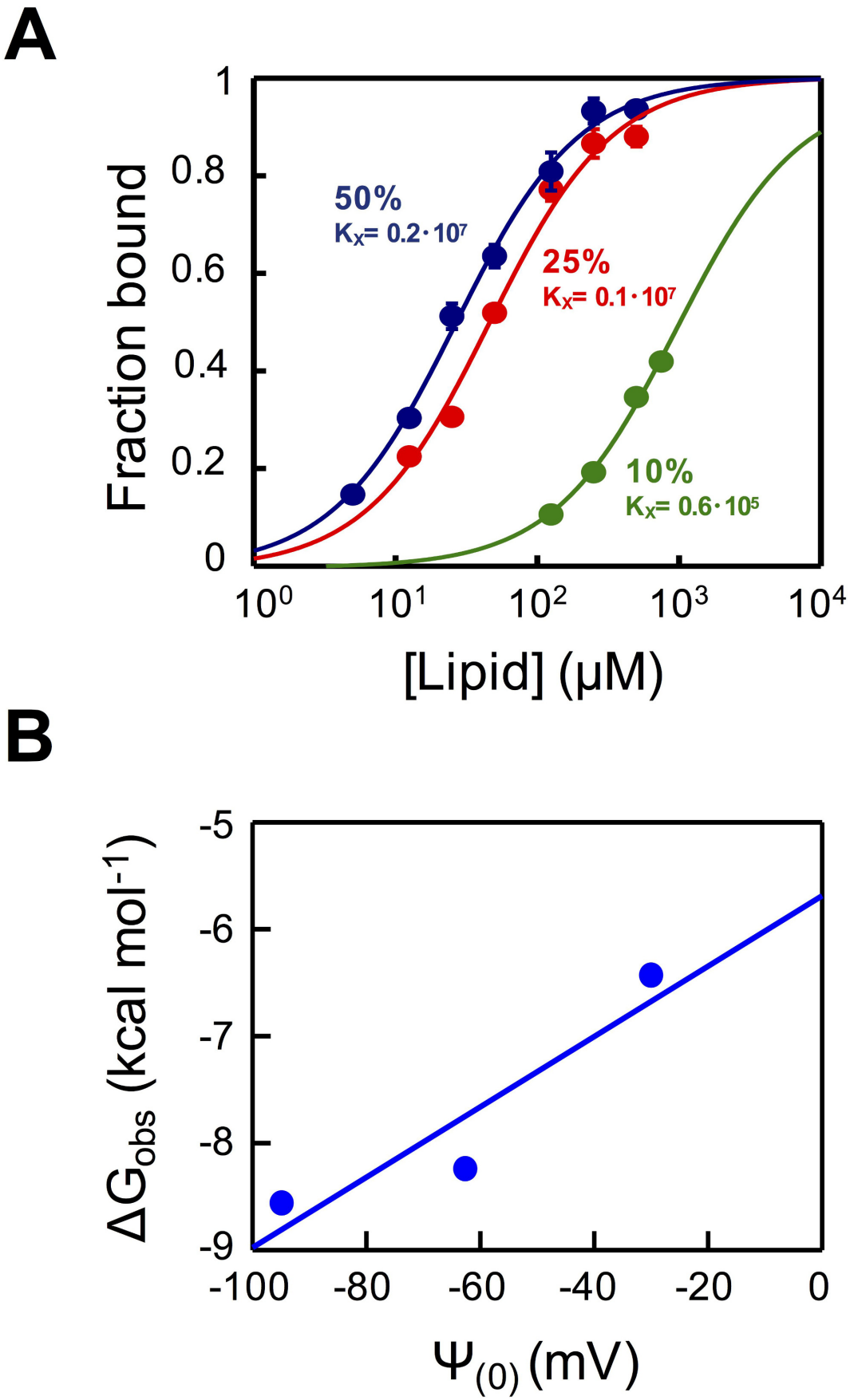

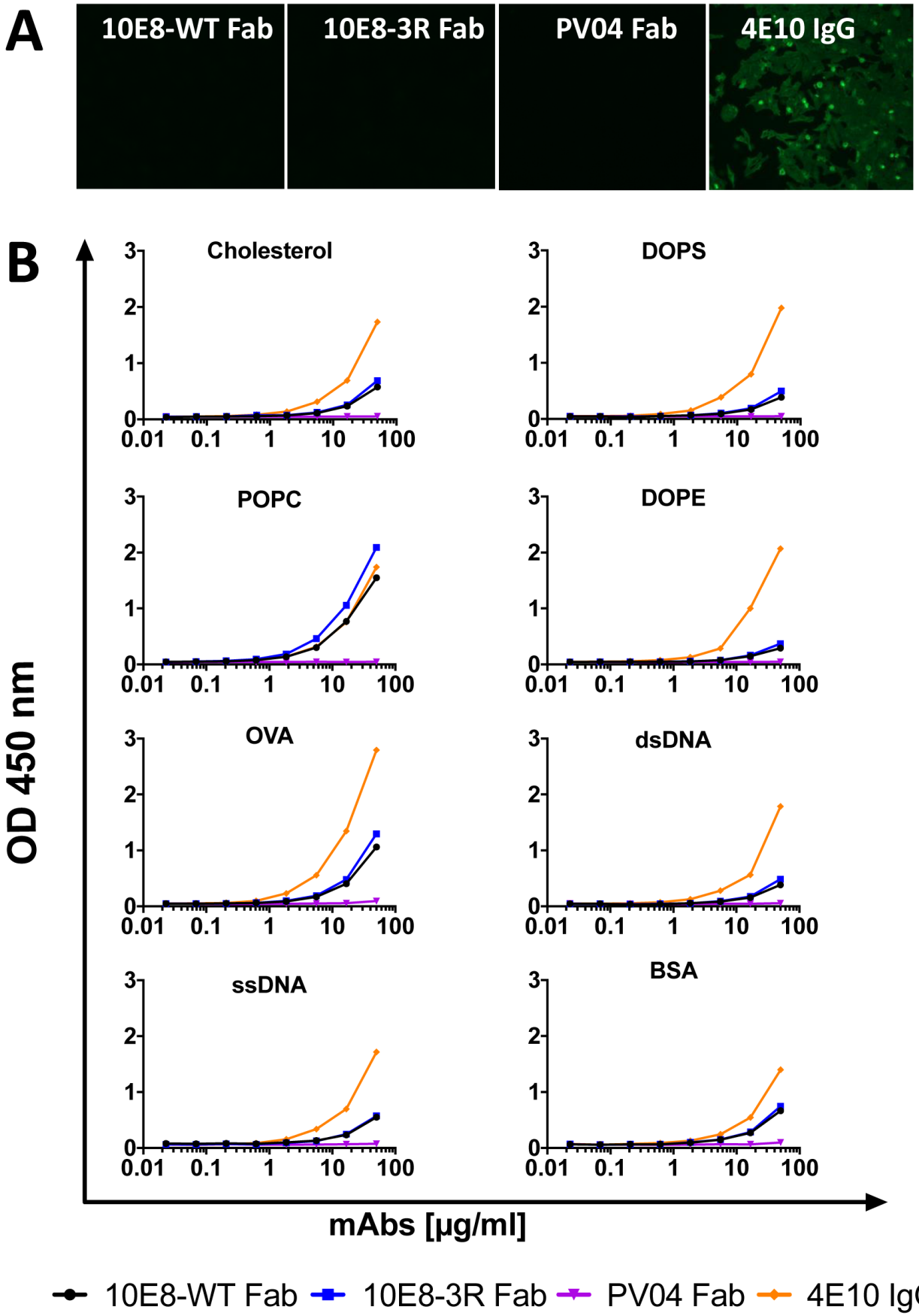

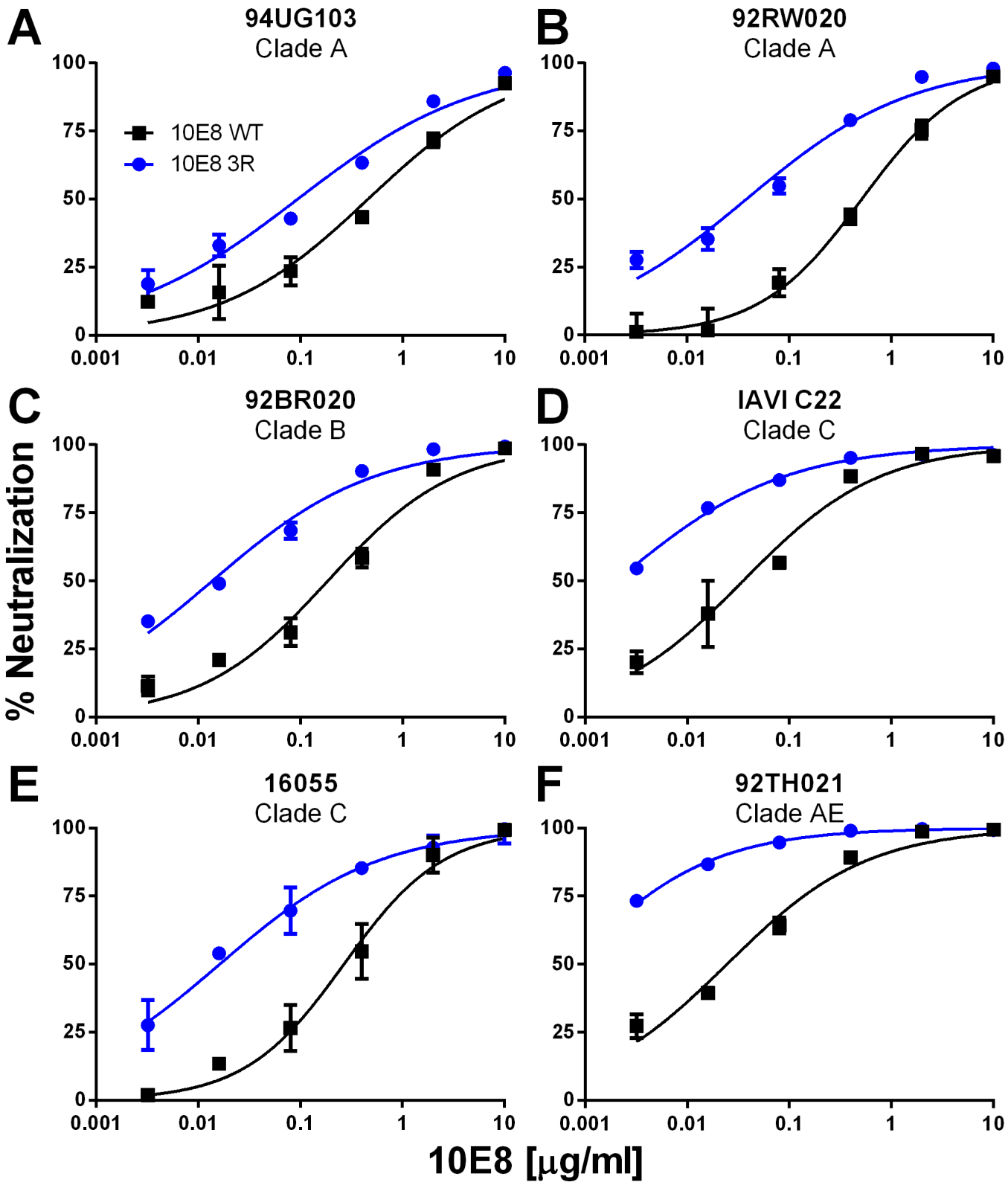




Journal of Virology

JVI

Journal of Virology